Journal of Advanced Research 23 (2020) 133–142

Contents lists available at ScienceDirect

Journal of Advanced Research

journal homepage: www.elsevier.com/locate/jare

Discovery of novel and potent $P2Y_{14}R$ antagonists *via* structure-based virtual screening for the treatment of acute gouty arthritis

Weiwei Wang [a,1], Chunxiao Liu [b,1], Hanwen Li [b], Sheng Tian [a,*], Yingxian Liu [a], Nanxi Wang [a], Duanyang Yan [a], Huanqiu Li [a,*], Qinghua Hu [b,*]

[a] Department of Medicinal Chemistry, College of Pharmaceutical Sciences, Soochow University, Suzhou 215123, China
[b] State Key Laboratory of Natural Medicines, China Pharmaceutical University, Nanjing 210009, China

HIGHLIGHTS

- A reliable Glide docking-based virtual screening (VS) pipeline for $P2Y_{14}R$ was developed.
- Several potent $P2Y_{14}R$ antagonists with novel scaffolds were identified utilizing the VS strategy.
- $P2Y_{14}R$ inhibitory effect was evaluated by testing cAMP levels in HEK293 cells.
- Anti-gout activity of screened compound was detected in MSU-treated THP-1 cells.
- The mechanism of test compound in treating acute gouty arthritis was elucidated.

GRAPHICAL ABSTRACT

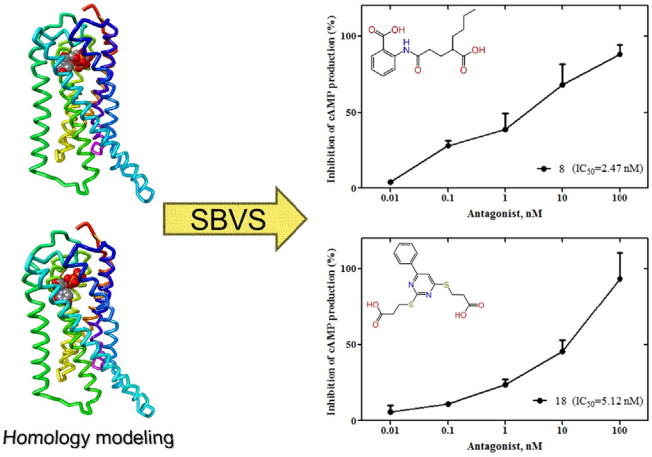

ARTICLE INFO

Article history:
Received 3 December 2019
Revised 23 January 2020
Accepted 11 February 2020
Available online 13 February 2020

Keywords:
$P2Y_{14}R$
Homology modeling
Virtual screening
Molecular docking
Pyroptosis
Acute gouty arthritis

ABSTRACT

$P2Y_{14}$ nucleotide receptor is a Gi protein-coupled receptor, which is widely involved in physiological and pathologic events. Although several $P2Y_{14}R$ antagonists have been developed thus far, few have successfully been developed into a therapeutic drug. In this study, on the basis of two $P2Y_{14}R$ homology models, Glide docking-based virtual screening (VS) strategy was employed for finding potent $P2Y_{14}R$ antagonists with novel chemical architectures. A total of 19 structurally diverse compounds identified by VS and drug-like properties testing were set to experimental testing. 10 of them showed good inhibitory effects against the $P2Y_{14}R$ (IC_{50} < 50 nM), including four compounds (compounds **8**, **10**, **18** and **19**) with IC_{50} value below 10 nM. The best VS hit, compound **8** exhibited the best antagonistic activity, with IC_{50} value of 2.46 nM. More importantly, compound **8** restrained monosodium uric acid (MSU)-induced pyroptosis of THP-1 cells through blocking the activation of Nod-like receptor 3 (NLRP3) inflammasome, which was attributed to its inhibitory effects on $P2Y_{14}R$-cAMP pathways. The key favorable residues uncovered using MM/GBSA binding free energy calculations/decompositions were detected and discussed. These findings

Peer review under responsibility of Cairo University.
* Corresponding authors.
E-mail addresses: stian@suda.edu.cn (S. Tian), huanqiuli@suda.edu.cn (H. Li), huqh@cpu.edu.cn (Q. Hu).
[1] These authors contributed equally to this study.

https://doi.org/10.1016/j.jare.2020.02.007
2090-1232/

suggest that the compound **8** can be used as a good lead compound for further optimization to obtain more promising $P2Y_{14}R$ antagonists for the treatment of acute gouty arthritis.

Introduction

The $P2Y_{14}$ receptor ($P2Y_{14}R$) is a member of P2-purigenic receptors, which has been regarded as inhibitory adenylate cyclae G-protein (Gi)-coupled receptor. It inhibits the production of 3′,5′-cyclicadenosine monophosphate (cAMP) through Gi protein, which could be activated by endogenous uidine diphosphate (UDP)-sugars. Activation of $P2Y_{14}R$ has been regarded to be associated with proinflammatory reactions, leading to neutrophil chemotaxis and mast cell degranulation [1–4]. $P2Y_{14}R$ is distributed among a variety of immune cells and is expressed in extensive tissues [5–7].

Several animal studies have demonstrated the value of $P2Y_{14}R$ as potential therapeutic target for recruitment of macrophages to liver, induction of insulin resistance in diabetes and local inflammation [8–10]. However, there are few studies focused on relationship between $P2Y_{14}R$ and acute gouty arthritis, which is a group of characteristic inflammatory reactions caused by innate immune disorders. Acute gouty arthritis is triggered by deposition of monosodium urate crystals (MSU) in the joint, resulting from the activation of Nod-like receptor 3 (NLRP3) inflammasome [11–13].

Our recent studies have showed that inhibition of NLRP3-mediated pyroptosis is a viable strategy for the prevention and treatment of acute gouty arthritis [14,15]. Till now, the treatment of gout still lacks the ideal drug. Previous study suggested that MSU can induce high expression of $P2Y_{14}R$ in human keratinocytes [16], offering strong evidence that $P2Y_{14}R$ might play causal role in MSU-related diseases. Meanwhile, the activation of $P2Y_{14}R$ is closely related to the content of intracellular cAMP, which was demonstrated to negatively regulate NLRP3 inflammasome [17], involved in inflammatory, diabetes, immune processes and other related complications [18,19]. Therefore, $P2Y_{14}R$ is likely to regulate the inflammatory response through NLRP3 inflammasome via cAMP in acute gouty arthritis.

To date, the current researches on $P2Y_{14}R$ antagonists only reported three types of compounds including pyrimidine piperidine, 2-naphthoic acid and 3-substituted benzoic acid [7,9,20–22]. Among them, the most active and selective $P2Y_{14}R$ antagonist is (4-(piperidin-4-yl)-phenyl)-7-(4-(trifluoromethyl)-phenyl)-2-naphthoic acid (PPTN, IC_{50} = 4 nM). However, the currently reported antagonists represented by 2-naphthoic acid suffered from poor solubility, low oral bioavailability, and high difficulty in synthesizing raw materials, bringing greater difficulties to further discussion of structure-activity relationship and biological evaluation [22]. In addition, based on $P2Y_{14}R$ homology models, a novel $P2Y_{14}R$ antagonists with scaffold, 3-(4-phenyl-1*H*-1,2,3-triazol-1-yl)-5-phenyl substituted benzoic acid was reported by Jacobson and coworkers using molecular docking and molecular dynamics (MD) simulation approaches. The identified $P2Y_{14}R$ antagonists showed quite acceptable binding affinities and the IC_{50} value of most potent $P2Y_{14}R$ antagonist was 31.7 nM. Based on these observations, there remains ongoing need to explore potent $P2Y_{14}R$ antagonists with novel chemical architectures. Besides, the development of promising $P2Y_{14}R$ antagonists could be a reasonable way for the treatment of gout.

Due to the high cost and time-consuming of high-throughput screening (HTS), virtual screening (VS) has aroused widespread concerns and been widely used in lead compound identifications of drug discovery [23,24]. For the crystal structures of $P2Y_{14}R$ has not yet been reported, the structure-based virtual screening (SBVS) can be used for finding novel $P2Y_{14}R$ antagonists with diverse chemical scaffolds based on well-established homology modes of $P2Y_{14}R$ [20–22].

To our knowledge, this is the first case to carry out a molecular docking strategy to massively screen a commercial library for finding novel $P2Y_{14}R$ antagonists based on $P2Y_{14}R$ homology models. Two well-prepared and minimized $P2Y_{14}R$ homology models (HM1 and HM2) [21] were used to screen the ChemDiv database. 19 diverse compounds were selected using drug-likeness properties prediction, REOS filtering, core scaffold clustering and purchased for biological testing. 10 of them (VS hit rate > 50%) exhibited significant antagonistic activity against $P2Y_{14}R$ (IC_{50} < 50-nM) and the most potent lead, compound **8** displayed a quite satisfactory antagonistic activity with IC_{50} value of 2.46 nM. Then, the feasibility of compound **8** as a drug candidate for treating gout treatment was investigated through a series of pharmacodynamics and mechanism of action. The results demonstrated that compound **8** restrained MSU-induced pyroptosis of THP-1 cells through blocking the activation of NLRP3 inflammasome, which was attributed to its inhibitory effects on P2Y14R-cAMP pathways. Finally, the Molecular Mechanics/Generalized Born Surface Area (MM/GBSA) binding free energy calculations/decompositions were employed to preliminarily detect the interaction patterns between $P2Y_{14}R$ and two most potent hits (compounds **8** and **18**). The key favorable residues for $P2Y_{14}R$ antagonists binding were detected and discussed. These findings may guide us to discovery more promising $P2Y_{14}R$ antagonists for treating acute gouty arthritis in the near future.

Materials and methods

$P2Y_{14}R$ homology models for docking-based virtual screening

The $P2Y_{14}R$ homology models (HM1 and HM2) [21] well established by Trujillo *et al.* were selected, optimized and applied in the Glide docking-based VS campaign of Schrödinger 9.0 software [25]. By utilizing the *Protein Preparation Wizard* module of Schrödinger 9.0, all water molecules were removed, the broken side chains were repaired and missing hydrogen atoms were added. Then, using the OPLS2005 force field, the partial charges and protonation states were assigned for each homology model.

Molecular docking-based virtual screening procedure

First of all, the *Receptor Grid Generation* module of Glide of Schrödinger 9.0 was used to generate binding site/pocket for molecular docking. The binding pocket size was set to 10 Å × 10 Å × 10 Å and centered on the centroid of the ligand in each $P2Y_{14}R$ homology model.

Then, the ChemDiv library including more than 2 million compounds was selected as screening database and screened against two $P2Y_{14}R$ homology models. Using the *LigPrep* mode of Glide, all compounds in the ChemDiv database were preprocessed carefully. For each compound in ChemDiv, the tautomers were generated at pH = 7.0 ± 2.0 and the different combinations of chiralities were also generated by setting the maximum number of stereoisomers to 32 by using *Epik*. At last, the final well-prepared ChemDiv database comprising more than 2.6 million compounds was set to Glide docking-based VS pipeline.

P2Y14R inhibitory activities screening

HEK293 cell lines stably expressing the $P2Y_{14}R$ were purchased from Keygen Biotech Co, ltd. Cells were plated in 384-well plates approximately 24 h before the assay at the density of 10,000 cells per well. Before assay, cells were briefly washed with phosphate-buffered saline solution to remove traces of serum and then incubated with 7.5 μL induction buffer contained 30 μM Forskolin (Med Chem Express, Cat. #HY-15371), 10 μM UDP-glucose (Sigma Aldrich, Cat. # U4625) and various concentrations of test compounds (0.01 nM, 0.1 nM, 1 nM, 10 nM, 100 nM) for 30 min at 37 °C, each concentration of 3 repetitions. $P2Y_{14}R$ inhibitory activities at each concentration were evaluated by detecting cAMP levels in order to calculate IC_{50} values.

Cell culture

THP-1 cell line purchased from American Type Culture Collection (Manassas, VA, USA) was cultured and stimulated with phorbol 12-myristate 13-acetate (PMA) as previous studies. Then, cells were pre-treated with Compound 8 or PPTN for 1 h, followed by the stimulation with MSU (500 μg/ml) for 12 h. Subsequently, the culture supernatants were collected for further investigation.

Measurements of IL-1β and cAMP

IL-1β concentrations in culture supernatants and cAMP levels in cell lysis were detected with ELISA Kit (Neobioscience, Shenzhen, China) or cAMP-Glo™ Assay Kit (Promega, WI, USA).

Pyroptosis assay

For pyroptosis analysis, active Caspase-1 and PI fluorescence of samples were measured using flow cytometry. Active caspase-1 was detected with FLICA 660 Caspase-1 Detection Kit (Immuno Chemistry Technologoes, USA), and propidium iodide (PI) staining was used to assess the integrity of cellular membrane.

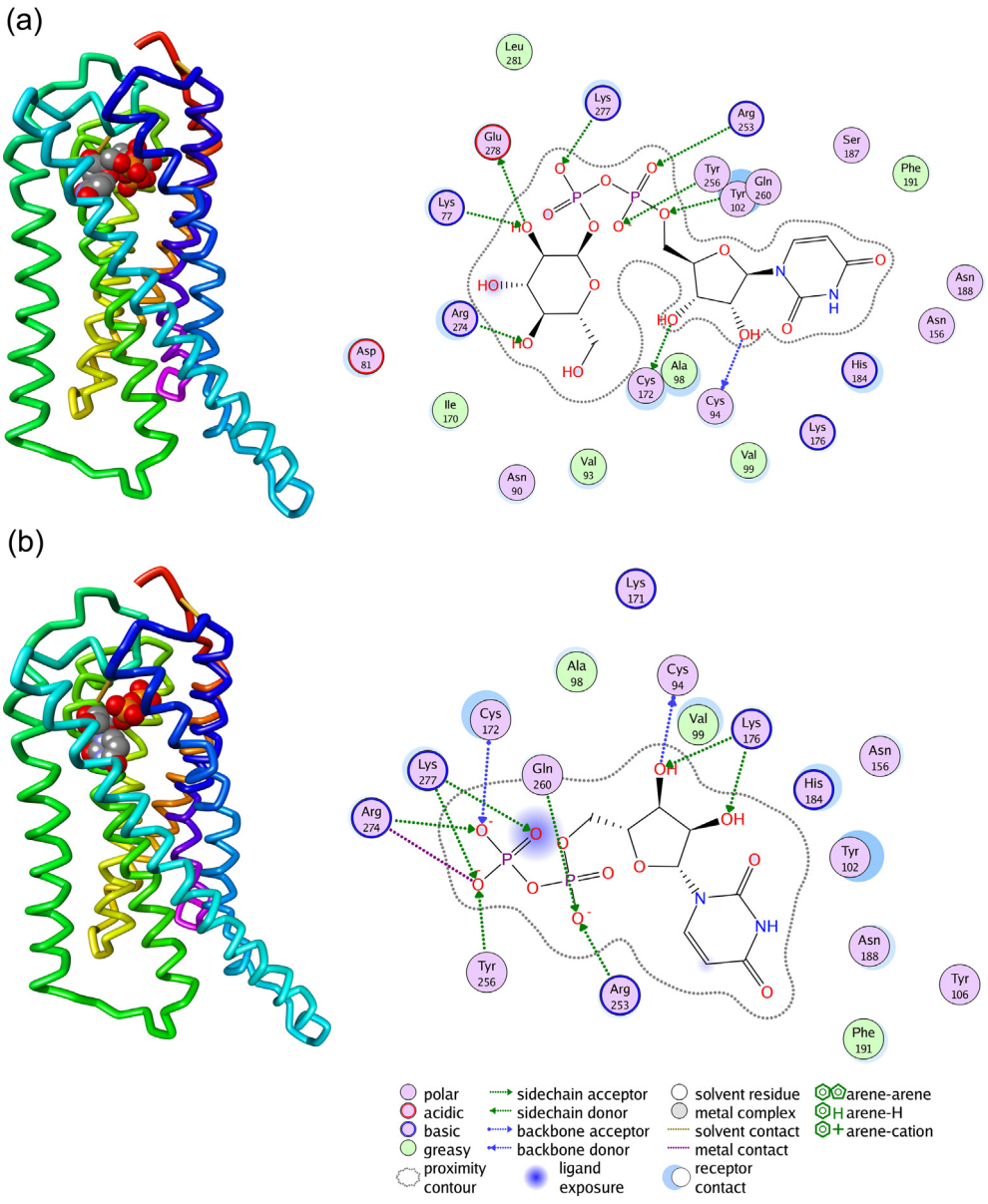

Fig. 1. The predicted binding poses and interaction patterns of (a) homology model 1 (HM1) and (b) homology model 2 (HM2) of P2Y14R. (The co-ligands in HM1 and HM2 are UDP-[1] glucose and UDP, respectively).

Immunofluorescence

After MSU stimulation, the cells were 4% paraformaldehyde fixed for 20–30 min. Permeabilization was performed with 0.3%–0.5% Triton X-100 for 20–30 min. When blocking for 1 h to avoid non-specific protein interactions, the samples were incubated with the primary antibody and secondary antibodies in sequence as previous studies. Fluorescent images were visualized by confocal laser scanning microscope (Fluoview, FV1000, Olympus, Japan).

Western blot

The THP-1 cells collected from each group were lysed in a RIPA buffer (Sigma, St. Louis, MO, USA). Samples containing approximately 50 mg protein was separated by 8–12% SDS-PAGE followed by the transference to polyvinylidene fluoride membranes (Millipore Corporation, MA, USA). Subsequently, PVDF membranes were treated with primary antibodies overnight at 4 °C after being blocked. The membranes were washed three times with Tris buffer

Table 1
Biological activities, representative molecular properties and key parameters identified in docking-based VS of the 19 purchased compounds from ChemDiv database.

Compd	ID_number[a]	IC_{50}(nM)	docking score[b]	MW	log*P*	log*S*	model
1	1278–0075	ND	−14.97	299.30	1.20	−2.29	HM1
2	1683–7093	35.4	−12.76	351.38	3.11	−4.46	HM1
3	2372–3546	ND	−16.34	303.29	2.18	−3.68	HM2
4	3473–2589	28.7	−14.39	349.43	3.54	−4.83	HM2
5	3975–0036	ND	−15.82	344.11	2.23	−4.00	HM2
6	4393–0019	45.5	−14.34	451.49	5.37	−6.67	HM1
7	5369–0063	16.5	−15.10	329.31	0.74	−2.13	HM2
8	6521–0066	2.46	−13.06	305.33	2.81	−3.79	HM1
9	7244–0067	18.6	−14.72	273.29	3.07	−2.40	HM2
10	8011–4760	5.35	−14.22	362.43	2.87	−5.92	HM1
11	8012–2120	ND	−12.98	389.42	3.77	−4.01	HM1
12	8013–6020	ND	−12.35	344.36	3.89	−4.31	HM1
13	8020–2337	ND	−14.06	231.17	1.21	−2.16	HM2
14	C301-4660	12.39	−15.15	387.46	2.50	−5.52	HM2
15	F293-0086	ND	−15.51	404.51	4.12	−4.81	HM2
16	F293-0205	ND	−14.64	438.53	4.51	−5.53	HM2
17	K783-4166	ND	−12.64	339.73	4.30	−5.62	HM1
18	Y040-3078	5.12	−13.60	314.34	3.90	−5.10	HM2
19	Y041-2308	7.71	−15.10	396.35	3.55	−5.82	HM1
20	PPTN[c]	2.74		475.50	3.80	−10.42	

[a] The compound number labeled in the ChemDiv database. According to the purity statements, the purity of all compounds purchased from the ChemDiv database is higher than 95%.
[b] The predicted binding affinity for compounds using the XP function based on HM1 or HM2 homology models.
[c] Positive control.

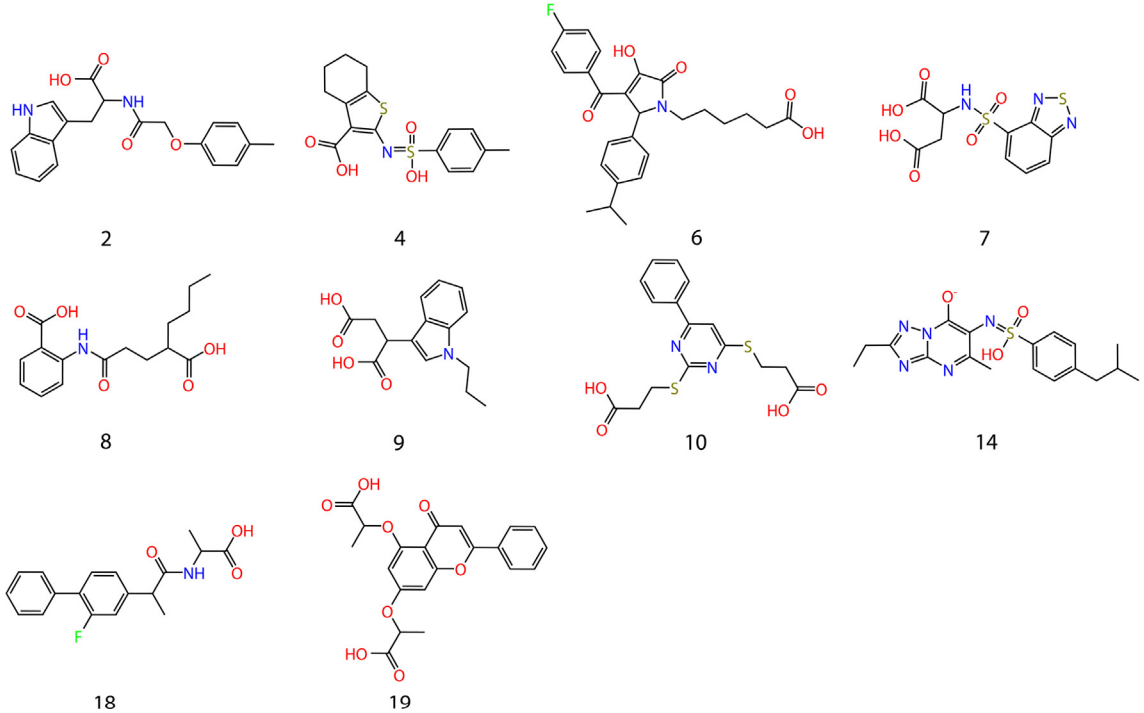

Fig. 2. Structures of 10 potent antagonists of $P2Y_{14}R$ (IC_{50} < 50 nM) identified from Glide docking-based VS.

saline-Tween20 (TBST), followed by incubation with appropriate horseradish peroxidase-conjugated secondary antibodies for 2 h. Finally, protein bands were visualized with an enhanced chemiluminescence (ECL) system (Keygen Biotech, China) and scanned with a Chemiluminescence gel imaging system (Tanon-5200Multi, China).

Statistical analysis

The data are expressed as mean values ± SDs. Data analyses were performed by one-way ANOVA with Tukey multiple comparison test (Graphpad Prism 7.0a), with $p < 0.05$ considered as significant.

Results and discussion

Molecular docking-based virtual screening pipeline

Two well-established $P2Y_{14}R$ homology models (HM1 and HM2) [21] proposed by Trujillo *et al.* were selected and minimized for the following docking-based virtual screening pipeline (Fig. 1). Three scoring functions of Glide docking (HTVS, SP XP) were applied to perform the sequential VS strategy [25]. The 50,000 highest -ranked compounds of the prepared ChemDiv database predicted by HTVS were re-docked using SP scoring mode. Then, the 5000 highest-ranked compounds of SP were re-calculated using the XP scoring function. At last, 1000 highest -ranked

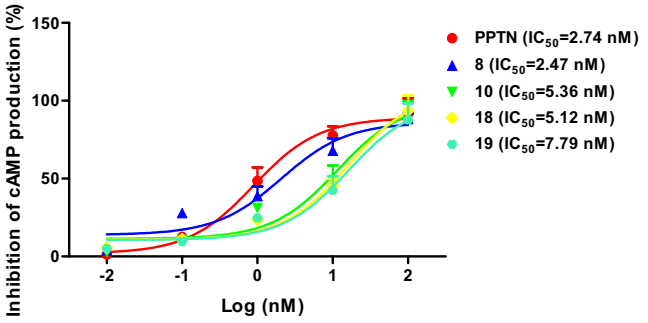

Fig. 3. Fluorescent assay of $P2Y_{14}R$ binding affinities (IC_{50} curves) of four identified $P2Y_{14}R$ antagonists (compounds **8**, **10**, **18** and **19**) with IC_{50} value below 10 nM, PPTN was run as positive control.

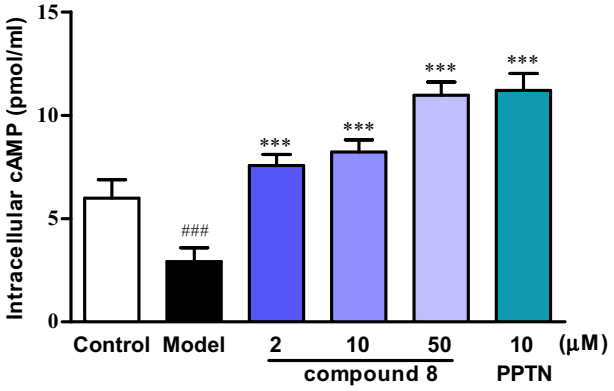

Fig. 5. Effects of compound **8** and PPTN on levels of cAMP in MSU-treated THP-1 cells. Compared with Control group: $^{###}P < 0.001$. Compared with Model group: $^{*}P < 0.05$, $^{**}P < 0.01$, $^{***}P < 0.001$. Each group (n = 4).

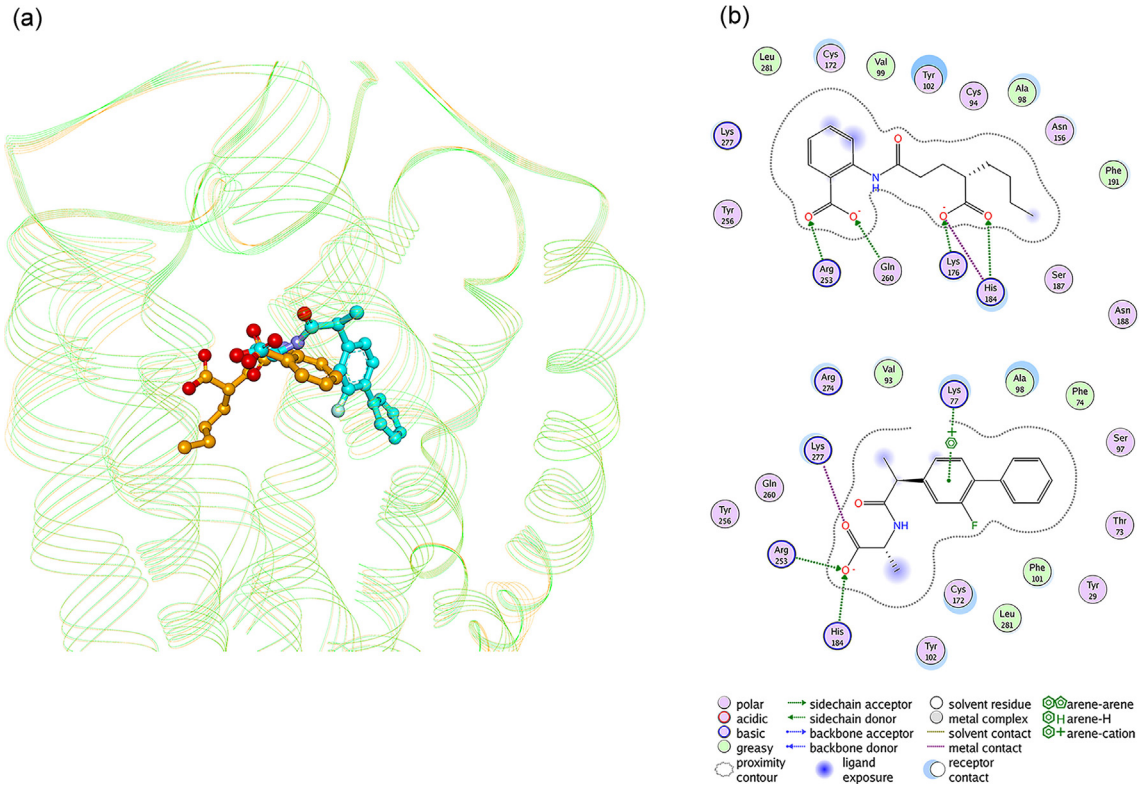

Fig. 4. (a) The predicted conformations of compounds **8** and **18** derived from Glide docking (the complexes of compound **8**-$P2Y_{14}R$ was colored in golden and compound **18**-$P2Y_{14}R$ was colored in green) and (b) predicted interaction patterns for compounds **8** and **18** in the binding pocket by applying HM1 and HM2 as docking structure, respectively. (For interpretation of the references to colour in this figure legend, the reader is referred to the web version of this article.)

compounds were obtained for each $P2Y_{14}R$ homology model. Followed by removing duplicates, Lipinski "Rule-of Five" filter [26] and drug-likeness models built in our previous studies [27–30], the compounds with reactive, undesirable functional groups or toxic were also deleted by applying REOS criterion [31]. Then, the compounds with less than two chiral centers were retained and then the remaining compounds were clustered using the *Tanimoto coefficient* evaluated based on *MACCS* structural keys (*Tanimoto coefficient* cut off value = 0.7). At last, 19 compounds were selected from ChemDiv database and purchased for experimental testing (Table 1).

In vitro $P2Y_{14}R$ inhibitory activities screening

$P2Y_{14}R$ inhibitory activities of testing compounds were determined based on production of cAMP in a HEK293 cell line stably expressing $P2Y_{14}R$. The results were listed in Table 1. As can be seen in Table 1, 10 of 19 purchased compounds (VS hit

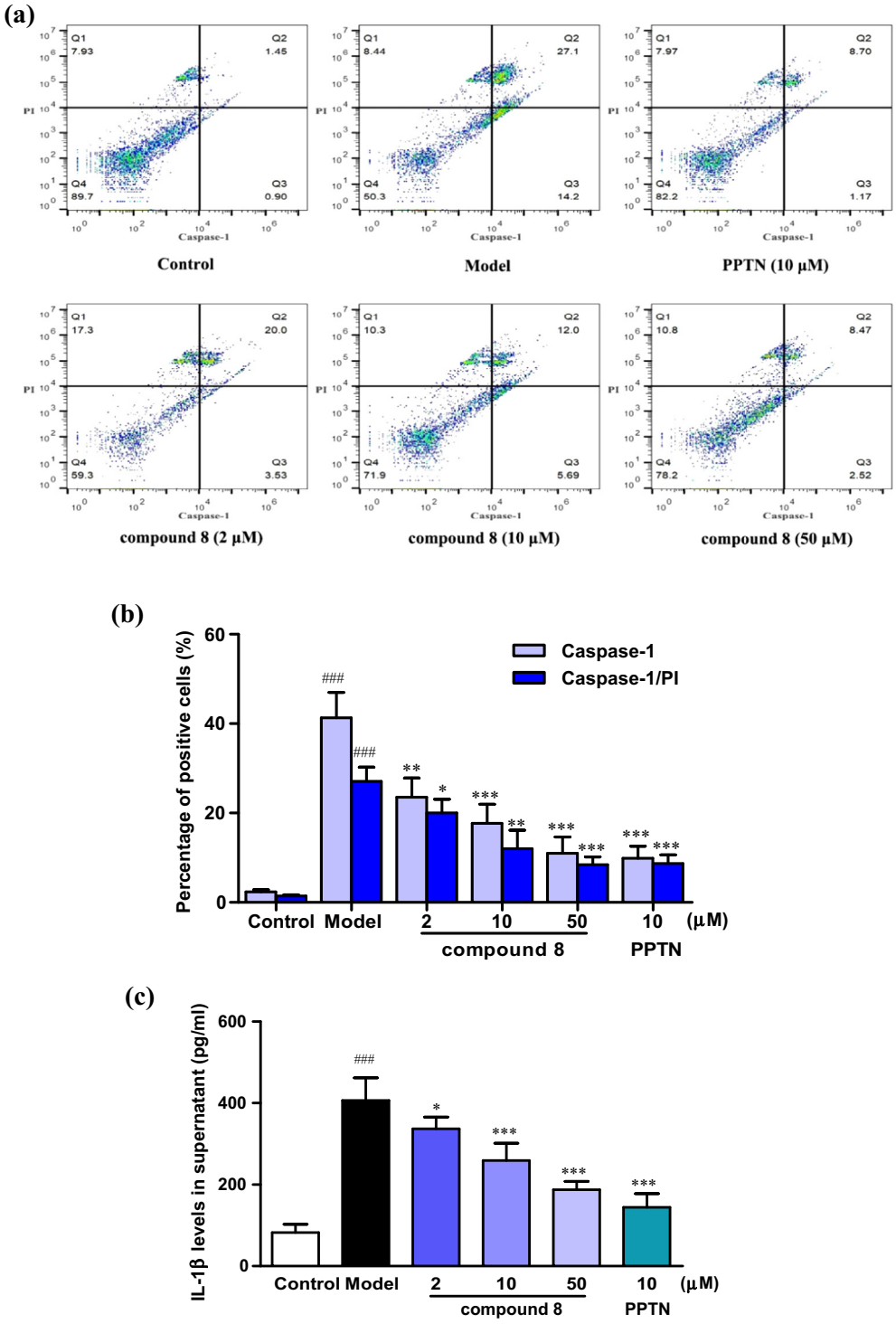

Fig. 6. Effects of compound **8** and PPTN on proportions of Caspase-1 single positive and Caspase-1/PI double positive cells (a and b), as well as levels of IL-1β (c) in cell culture supernatants of MSU-treated THP-1 cells. Compared with Control group: $^{###}P < 0.001$. Compared with Model group: $^{*}P < 0.05$, $^{**}P < 0.01$, $^{***}P < 0.001$. Each group (n = 4).

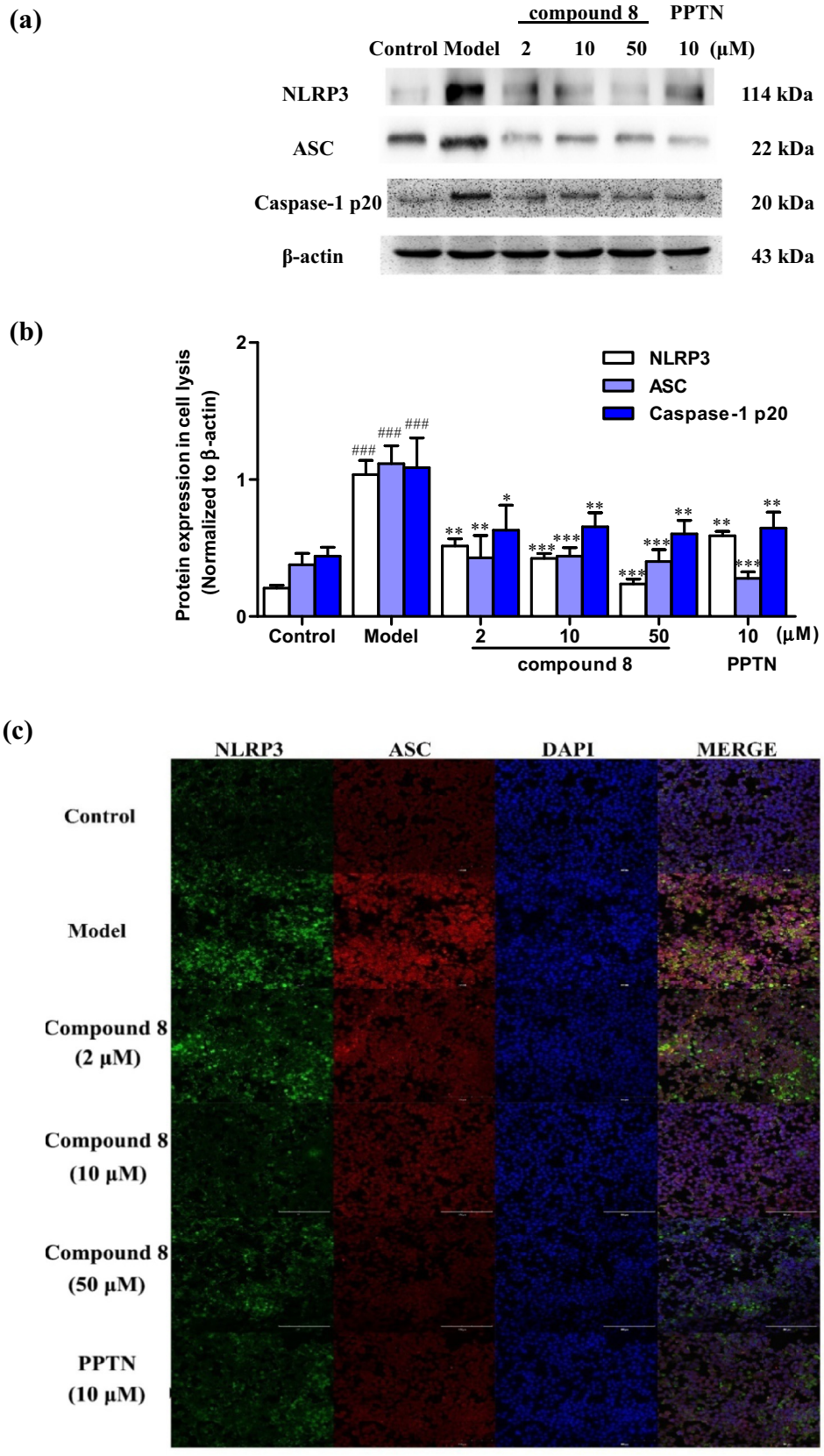

Fig. 7. Effects of compound **8** and PPTN on protein expressions of NLRP3, ASC and Caspase-1 (p20) (a and b) in MSU-treated THP-1 cells. Compared with Control group: $^{###}P < 0.001$. Compared with Model group: $^{*}P < 0.05$, $^{**}P < 0.01$, $^{***}P < 0.001$. Each group (n = 4). Representative confocal microscopy photographs of THP-1 cells with immunofluorescence changes are presented (c).

rate = 52.63%) showed quite acceptable inhibitory activity (IC_{50} < 50 nM) for $P2Y_{14}R$. The chemical structures of 10 identified $P2Y_{14}R$ antagonists with IC_{50} value below 50 nM are shown in Fig. 2 and those of the remaining compounds were shown in the Fig. S1 in the Supporting Information. Among them, four compounds (compound **8**, **10**, **18** and **19**) exhibited satisfactory antagonistic activity of $P2Y_{14}R$ (IC_{50} value below 10 nM, Fig. 3), and compound **8** showed the most potent antagonistic activity (IC_{50} = 2.46 nM). The schematic representations of the predicted binding poses and interaction patterns between the $P2Y_{14}R$ and the two most potent identified antagonists (compounds **8** and **18**) are depicted in Fig. 4.

In vitro anti-inflammatory effects of compound 8 through regulation of cAMP and NLRP3 inflammasome

As shown in Fig. 5, cAMP concentrations were significantly decreased after MSU stimulation, which was reversed by pre-treatment of compound **8** and PPTN. More importantly, MSU administration led to a significant increase in the proportion of pyroptotic cells characterized by Caspase-1/PI double positive staining analyzed by flow cytometry. As expected, this alternation was also improved in compound **8** and PPTN treated cells (Fig. 6a and b). Consistently, IL-1β levels in the supernatant of THP-1 cell culture medium were obviously increased in model group. Both compound **8** and PPTN interventions apparently inhibited the release of IL-1β, reflecting the mitigation of inflammation caused by MSU (Fig. 6c). As shown in Fig. 7, protein expressions of NLRP3, ASC (apoptosis-associated speck-like protein containing a CARD) and Caspase-1 p20 were apparently increased in THP-1 cells with MSU stimulation. And aforementioned alterations were reversed by pre-treatment of compound **8** and PPTN.

On the other hand, inhibitory effect of compound **8** on NLRP3 inflammasome was also confirmed by immunofluorescence data (Fig. 7c). When compared to control cells, model cells apparently showed higher fluorescence intensity in NLRP3 and ASC staining without observed difference in DAPI (4′,6-diamidino-2-phenylin dole) intensity.

Primary structure-activity relationship discussions using MM/GBSA free energy decompositions

For exploring the detected antagonistic activity differences, the most potent VS hits (compounds **8** and **18**) of $P2Y_{14}R$ were selected

Table 2
The predicted binding free energies using MM/GBSA rescoring of compounds 8 and 18.

Compd	Polar contributions		Nonpolar contributions		ΔG_{pred}[e]
	ΔE_{ele}[a]	ΔG_{GB1}[b]	ΔE_{vdw}[c]	ΔG_{SA}[d]	
8	−698.72	699.19	−36.92	−6.40	−42.85
18	−388.98	373.62	−39.38	−6.46	−61.20

[a] Electrostatic contribution.
[b] Polar part of desolvation.
[c] Van der Waals contribution.
[d] Non-polar part of desolvation.
[e] The predicted total binding energies using MM/GBSA calculations.

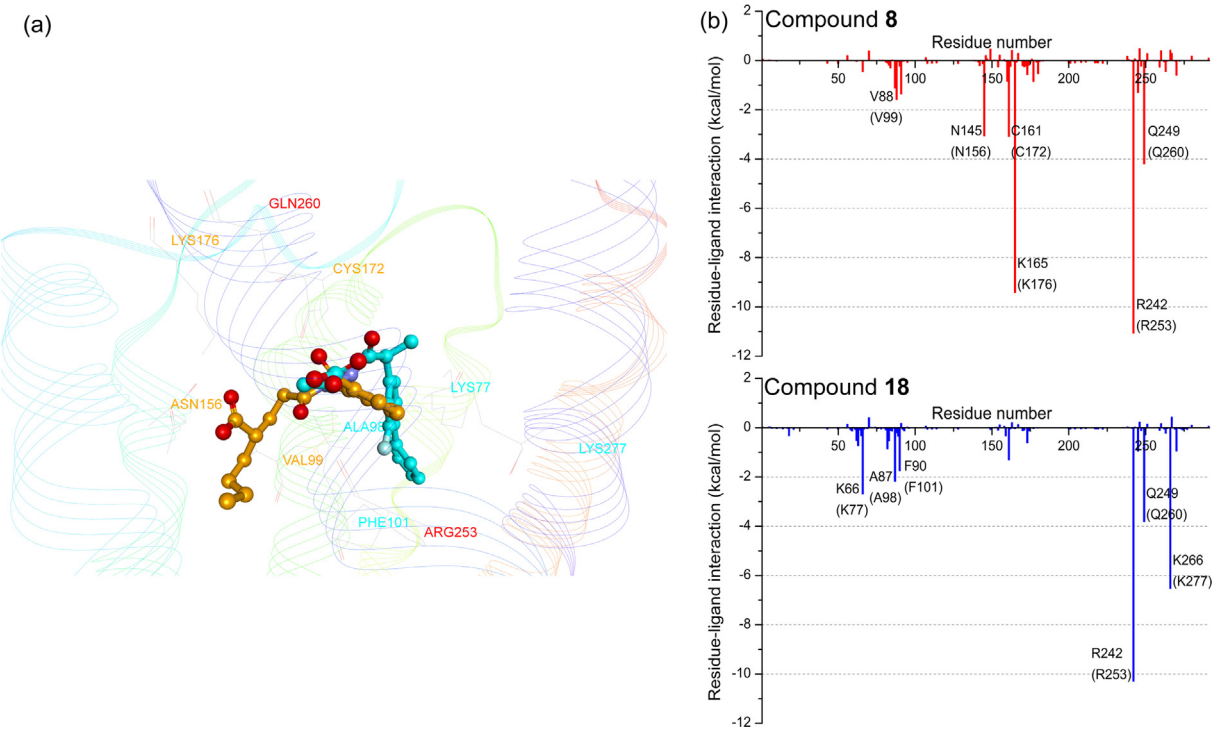

Fig. 8. (a) The binding poses of compounds **8** and **18** optimized from the MM/GBSA calculations (the favorable residues for compounds **8** and **18** binding with $P2Y_{14}R$ are colored in golden and green, respectively. The same key residues for two compounds are colored in red), (b) the antagonist-residues interaction spectra of compounds **8** and **18**.

and docked into the respectively binding pocket of $P2Y_{14}R$ homology models (HM1 and HM2) using *Glide* XP scoring mode. In order to investigate the interaction pattern between PPTN and P2Y14 receptor, the PPTN was docked into the binding pocket of HM1 and HM2 using SP and XP scoring modes of Glide docking. The docking results demonstrated that PPTN cannot produce acceptable docking poses against P2Y14 receptor. Considering the higher protein flexibility of P2Y14 receptor, the PPTN may adopt quite distinct binding mode with P2Y14 receptor, compared with assayed compounds in our study.

By employing the MM/GBSA approach [32–34], the predicted binding poses of compounds **8** and **18** interacting with $P2Y_{14}R$ were optimized and rescored. The predicted total binding free energies using MM/GBSA rescoring of compounds **8** and **18** were −42.85 and −61.20 kcal/mol, respectively (Table 2). Then, for quantitatively discerning the contribution of each key residues of $P2Y_{14}R$ binding with compounds **8** and **18**, the antagonist-residues interaction spectra were depicted and analyzed. As can be seen in Fig. 8a, two most potent antagonists of $P2Y_{14}R$ have quite distinct binding sites in the binding pocket of $P2Y_{14}R$. For example, the residues ofVal99, Asn156, Cys172, Lys176, Arg253 and Gln260 play as the key residues for the compound **8** binding with $P2Y_{14}R$, and their favorable contributions to the total binding energy (ΔG_{pred}) are all lower than −1.5 kcal/mol. Compared with compound **8**, compound **18** has quite different favorable binding residues. The dominant residues of compound **18** interacting with $P2Y_{14}R$ are Lys77, Ala98, Phe101, Arg253, Gln260 and Lys277. The same key residues for compounds **8** and **18** binding with $P2Y_{14}R$ are Arg253 and Gln260. The energy contributions of Arg253 and Gln260 for compounds **8** were −11.07 and −4.20 kcal/mol (Fig. 8a), and those for compound **18** were −10.30 and −3.82 kcal/mol (Fig. 8b), respectively. Considering inherent high flexibility of $P2Y_{14}R$ structure, we found that maintaining stable/strong interactions with these favorable residues (Lys77, Ala98, Val99, Phe101, Asn156, Cys172, Lys176, Arg253, Gln260 and Lys277) are the requirements for obtaining promising $P2Y_{14}R$ antagonists. This finding will provide some clues to design/develop more optimal antagonists of $P2Y_{14}R$ in the lead optimization stage.

Conclusions

In the current work, we adopted Glide docking-based virtual screening strategy for finding potent $P2Y_{14}R$ antagonists using two well-established $P2Y_{14}R$ homology models. 19 potential hits with quite novel chemical scaffolds were set to antagonistic activity testing. 10 of them revealed significant antagonistic activity against $P2Y_{14}R$. The IC_{50} of the most potent identified $P2Y_{14}R$ antagonist (compound **8)** can reach 2 nM, which was higher than the previously reported 2-naphthoic acid compound PPTN. To further confirm its feasibility as a drug for the prevention and treatment of acute gouty arthritis, we established a THP-1 cell model exposed to MSU to simulate acute gouty arthritis. The results demonstrated that compound **8** can significantly restore cAMP production and reduce IL-1β secretion. More importantly, compound **8** blocked the pyroptosis of THP-1 cells and inhibited the activation of NLRP3 inflamasome. These findings indicate that the compound **8** might be applied as a good lead compound for further modification/optimization for the treatment of acute gouty arthritis.

Compliance with ethics requirements

This article does not contain any studies with human or animal subjects.

Declaration of Competing Interest

The authors declared that they have no conflicts of interest to this work.

We declare that we do not have any commercial or associative interest that represents a conflict of interest in connection with the work submitted.

Acknowledgements

This study was supported by Natural Science Foundation of Jiangsu Province (Grant No. BK2011437), the National Natural Science Foundation of China (81773745 and 81502982), "Double First-Class" University project of China Pharmaceutical University (CPU2018GF02), the Priority Academic Program Development of the Jiangsu Higher Education Institutes (PAPD) and the Jiangsu Key Laboratory of Translational Research for Neuropsychiatric Diseases (BM2013003). We are grateful to Prof. Youyong Li in the Institute of Functional Nano & Soft Materials (FUNSOM) at Soochow University for providing Schrödinger software package for molecular docking.

Appendix A. Supplementary material

Supplementary data to this article can be found online at https://doi.org/10.1016/j.jare.2020.02.007.

References

[1] Gendaszewska-Darmach E, Weglowska E, Walczak-Drzewiecka A, Karas K. Nucleoside 5 '-O-monophosphorothioates as modulators of the P2Y14 receptor and mast cell degranulation. Oncotarget 2016;7(43):69358–70.
[2] Sesma JI, Livraghi-Butrico A, Wilkinson KJ, Weitzer C, Saini Y, Harden T, et al. Blockage of the P2y14-receptor inhibits neutrophil infiltration in chronic lung diseases. Am J Respir Crit Care Med 2015;191.
[3] Gao Z-G, Ding Y, Jacobson KA. UDP-glucose acting at P2Y(14) receptors is a mediator of mast cell degranulation. Biochem Pharmacol 2010;79(6):873–9.
[4] Azroyan A, Cortez-Retamozo V, Bouley R, Liberman R, Ruan YC, Kiselev E, et al. Renal intercalated cells sense and mediate inflammation via the P2Y(14) receptor. PLoS ONE 2015;10(3).
[5] Ko H, Fricks I, Ivanov AA, Harden TK, Jacobson KA. Structure-activity relationship of uridine 5'-diphosphoglucose analogues as agonists of the human P2Y(14) receptor. J Med Chem 2007;50(9):2030–9.
[6] Das A, Ko H, Burianek LE, Barrett MO, Harden TK, Jacobson KA. Human P2Y(14) receptor agonists: truncation of the hexose moiety of uridine-5 '-diphosphoglucose and its replacement with alkyl and aryl groups. J Med Chem 2010;53(1):471–80.
[7] Gauthier JY, Belley M, Deschenes D, Fournier J-F, Gagne S, Gareau Y, et al. The identification of 4,7-disubstituted naphthoic acid derivatives as UDP-competitive antagonists of P2Y(14). Bioorg Med Chem Lett 2011;21(10):2836–9.
[8] Barrett MO, Sesma JI, Ball CB, Jayasekara PS, Jacobson KA, Lazarowski ER, et al. A selective high-affinity antagonist of the P2Y(14) receptor inhibits UDP-glucose-stimulated chemotaxis of human neutrophils. Mol Pharmacol 2013;84(1):41–9.
[9] Kiselev E, Barrett MO, Katritch V, Paoletta S, Weitzer CD, Brown KA, et al. Exploring a 2-naphthoic acid template for the structure-based design of P2Y(14) receptor antagonist molecular probes. ACS Chem Biol 2014;9(12):2833–42.
[10] Schlaich T, Zech A, Wiesler B, Hobfeld M, Idzko M. P2y14 receptor deficiency attenuates phenotype of allergic airway inflammation in mice. Am J Respir Crit Care Med 2016;193.
[11] Kingsbury SR, Conaghan PG, McDermott MF. The role of the NLRP3 inflammasome in gout. J Inflammation Res 2011;4:39–49.
[12] Wu H, Zhou M, Lu G, Yang Z, Ji H, Hu Q. Emodinol ameliorates urate nephropathy by regulating renal organic ion transporters and inhibiting immune inflammatory responses in rats. Biomed Pharmacother 2017;96:727–35.
[13] Martin WJ, Shaw O, Liu X, Steiger S, Harper JL. Monosodium urate monohydrate crystal-recruited noninflammatory monocytes differentiate into M1-like proinflammatory macrophages in a peritoneal murine model of gout. Arthritis Rheum 2011;63(5):1322–32.
[14] Huang J, Zhou Z, Zhou M, Miao M, Li H, Hu Q. Development of benzoxazole deoxybenzoin oxime and acyloxylamine derivatives targeting innate immune sensors and xanthine oxidase for treatment of gout. Biorg Med Chem 2018;26(8):1653–64.

[15] Yang M, Teng G, Li G, Huang T, Xu R. Effectiveness of osthole on uric acid crystal-induced acute gouty arthritis through the inhibition of NLRP3 inflammasome. Int J Pharmacol 2018;14(8):1169–78.
[16] Uratsuji H, Tada Y, Hau CS, Shibata S, Kamata M, Kawashima T, et al. Monosodium urate crystals induce functional expression of P2Y(14) receptor in human keratinocytes. J Invest Dermatol 2016;136(6):1293–6.
[17] Chen Y, Le TH, Du Q, Zhao Z, Liu Y, Zou J, et al. Genistein protects against DSS-induced colitis by inhibiting NLRP3 inflammasome via TGR5-cAMP signaling. Int Immunopharmacol 2019;71:144–54.
[18] Lu R, Zhang Z, Jiang C. Recent progress on the discovery of P2Y(14) receptor antagonists. Eur J Med Chem 2019;175:34–9.
[19] Lazarowski ER, Harden TK. UDP-sugars as extracellular signaling molecules: cellular and physiologic consequences of P2Y(14) receptor activation. Mol Pharmacol 2015;88(1):151–60.
[20] Junker A, Balasubramanian R, Ciancetta A, Uliassi E, Kiselev E, Martiriggiano C, et al. Structure-based design of 3-(4-Aryl-1H-1,2,3-triazol-1-yl)-biphenyl derivatives as P2Y(14) receptor antagonists. J Med Chem 2016;59 (13):6149–68.
[21] Trujillo K, Paoletta S, Kiselev E, Jacobson KA. Molecular modeling of the human P2Y(14) receptor: A template for structure-based design of selective agonist ligands. Biorg Med Chem 2015;23(14):4056–64.
[22] Yu J, Ciancetta A, Dudas S, Duca S, Lottermoser J, Jacobson KA. Structure-guided modification of heterocyclic antagonists of the P2Y(14) receptor. J Med Chem 2018;61(11):4860–82.
[23] Hou TJ, Xu XJ. Recent development and application of virtual screening in drug discovery: An overview. Curr Pharm Des 2004;10(9):1011–33.
[24] Bajorath F. Integration of virtual and high-throughput screening. Nat Rev Drug Discovery 2002;1(11):882–94.
[25] Schrödinger, version 9.0, Schrödinger, LLC, New York, NY, 2009, http://www.schrodinger.com.
[26] Lipinski CA, Lombardo F, Dominy BW, Feeney PJ. Experimental and computational approaches to estimate solubility and permeability in drug discovery and development settings. Adv Drug Del Rev 1997;23(1–3):3–25.
[27] Tian S, Wang J, Li Y, Li D, Xu L, Hou T. The application of in silico drug-likeness predictions in pharmaceutical research. Adv Drug Del Rev 2015;86:2–10.
[28] Tian S, Wang J, Li Y, Xu X, Hou T. Drug-likeness analysis of traditional Chinese medicines: prediction of drug-likeness using machine learning approaches. Mol Pharm 2012;9(10):2875–86.
[29] Tian S, Li Y, Wang J, Zhang J, Hou T. ADME evaluation in drug discovery. 9. Prediction of oral bioavailability in humans based on molecular properties and structural fingerprints. Mol Pharm 2011;8(3):841–51.
[30] Zhu F, Wang Y, Du Q, Ge W, Li Z, Wang X, et al. Structural optimization of aminopyrimidine-based CXCR4 antagonists. Eur J Med Chem 2020;187. 111914.
[31] Walters WP, Stahl MT, Murcko MA. Virtual screening - an overview. Drug Discovery Today 1998;3(4):160–78.
[32] Wang E, Sun H, Wang J, Wang Z, Liu H, Zhang JZH, et al. End-point binding free energy calculation with MM/PBSA and MM/GBSA: strategies and applications in drug design. Chem Rev 2019;119(16):9478–508.
[33] Lu W, Zhang D, Ma H, Tian S, Zheng J, Wang Q, et al. Discovery of potent and novel smoothened antagonists via structure-based virtual screening and biological assays. Eur J Med Chem 2018;155:34–48.
[34] Tian S, Wang X, Li L, Zhang X, Li Y, Zhu F, et al. Discovery of novel and selective adenosine A(2A) receptor antagonists for treating Parkinson's disease through comparative structure-based virtual screening. J Chem Inf Model 2017;57 (6):1474–87.